ELSEVIER

Nuclear Engineering and Design 220 (2003) 105–118

Nuclear Engineering and Design

www.elsevier.com/locate/ned

Shear transfer constitutive model for pre-cracked RC plate subjected to combined axial and shear stress

Katsuhiko Umeki [a,*], Yoshio Kitada [b], Takao Nishikawa [c], Koichi Maekawa [d], Mamoru Yamada [e]

[a] *Nuclear Facilities Division, Obayashi Corporation, 1-19-9, Tsutsumi-Dori, Sumida-ku, Tokyo 131-8510, Japan*
[b] *Seismic Engineering Center, Nuclear Power Engineering Corporation, Tokyo, Japan*
[c] *Graduate School of Engineering, Tokyo Metropolitan University, Tokyo, Japan*
[d] *Department of Civil engineering, The University of Tokyo, Tokyo, Japan*
[e] *Technical Research Institute, Obayashi Corporation, Tokyo, Japan*

Received 10 August 2001; received in revised form 19 April 2002; accepted 12 August 2002

Abstract

This paper proposes the constitutive model for the shear transfer through the cracks of pre-cracked reinforced concrete (RC) plate subjected to combined axial and shear stress. The plate is a scale model of a shear wall of a nuclear power plant (NPP) building. Twelve plate specimens were initially cracked and then loaded to the failure point by increasing cyclic shear under constant axial stress. Tangential shear modulus, G_{cr}, values are estimated from the $v-\gamma$ relationships observed in the test results and formulated to the constitutive model as the correlation function of the normal strain perpendicular to the crack plane, ε_{cr}, and shear strain, γ_{cr}, based on the smeared crack model concept. By incorporating the proposed model to a nonlinear FEM analysis program and comparing the analysis results with the test results, it is apparent that the program could be improved in its analytical accuracy. The proposed model will be useful for the nonlinear analysis of RC shear walls when the walls are exposed to simultaneous multi-directional load.

1. Introduction

Since a seismic input motion is three directional, response of the building is also three directional. For example, in an NPP building a reinforced concrete (RC) shear wall in the East–West (EW) direction works as a 'flange' that bears an axial load, when the building is struck in the 'North–South' (NS) direction. This same shear wall will turn into a 'web' that bears a shear load, when the building is struck in the orthogonal EW direction. Once the cracks are generated in a shear wall, its stiffness would decrease and this smaller stiffness would remain even when the building is struck in the other directions. In other words, the nonlinear stiffness behavior of shear walls depends on their seismic responses in the three directions, not just in a typical direction.

* Corresponding author. Tel.: +81-3-5247-8552; fax: +81-3-5247-8683
E-mail address: umeki.katsuhiko@obayashi.co.jp (K. Umeki).

0029-5493/02/$ - see front matter
PII: S0029-5493(02)00292-3

In the current seismic design in Japan, for example, although the horizontal seismic design forces in the NS and EW directions are evaluated from nonlinear response analyses in two directions, respectively, interactions between the responses are not considered. In order to evaluate the seismic design forces reasonably, analyses considering those interactions should be conducted. For that objective, a constitutive model for shear transfer through existing cracks should be provided. However, since such a constitutive model has not been proposed yet, development of the model has been the important technical theme.

The nuclear power engineering corporation (NUPEC) of Japan started the project, 'model test of multi-axis loading on RC shear walls,' in 1994. The test on the shear transfer through existing bending cracks is taken as the scope of the project. Basically, the shear transfer behavior is a highly nonlinear problem that depends on normal and shear stresses induced on cracks. To date, several researchers have tried to clarify the behavior. Their study seemed to focus on the basic behavior of cracks, not the shear wall behavior of nuclear power plant (NPP) buildings.

So, this study aims at developing the constitutive model for shear transfer through the cracks at shear walls of the NPP building (Kitada et al., 1999; Habasaki et al., 2000).

2. Test specimen

2.1. Test parameters

Test parameters are listed in Table 1. They were selected based on the survey of actual NPP building designs. The variation of reinforcement ratio was given by the different size of applied rebar in diameters as D13, 16 and 22. The axial stress variations, which occur during an earthquake, were given by the several levels of constant axial stress to develop a constitutive model. The levels were determined in the range from a 3.0 MPa in compression to a 3.0 MPa in tension based on the actual plant condition.

Table 1
Test specimen and parameter

f_0 axial stress (MPa)	ρ_n (%)		
	0.84 (D13)	1.32 (D16)	2.58 (D22)
−2.94 [−3.0]		○	
−1.47 [−1.5]	○	○	○
0.0 (0.0)	○	○	○
+0.73 [0.75]		○	
+1.47 [1.5]	○	○	○
+2.94 [3.0]		○	

[ ] Name of test specimen; −, axial compression; +, axial tension.

2.2. Dimensions of the test specimen

Test specimens are the square RC plates of $1.2 \times 1.2 \times 0.2$ m as shown in Fig. 1. The size is about 1/5 the scale of a typical RC shear wall in an NPP building. Each specimen has some loading rods at the four sides to which axial and shear loads are applied. The outside of the specimen was strengthened by steel plate pads to prevent a local failure.

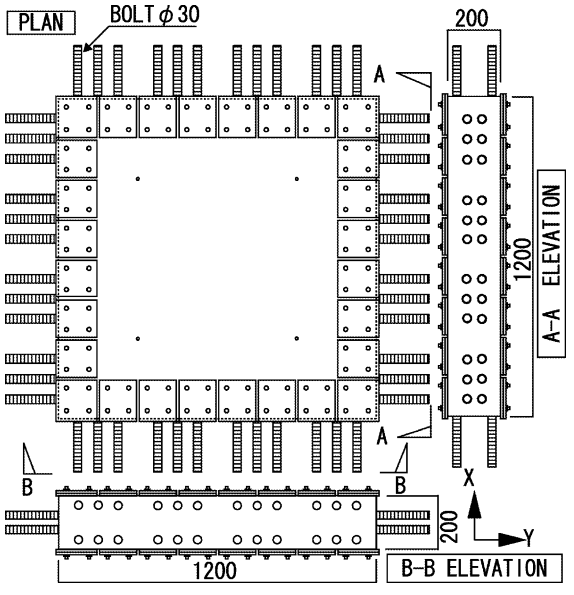

Fig. 1. Configuration of test specimen.

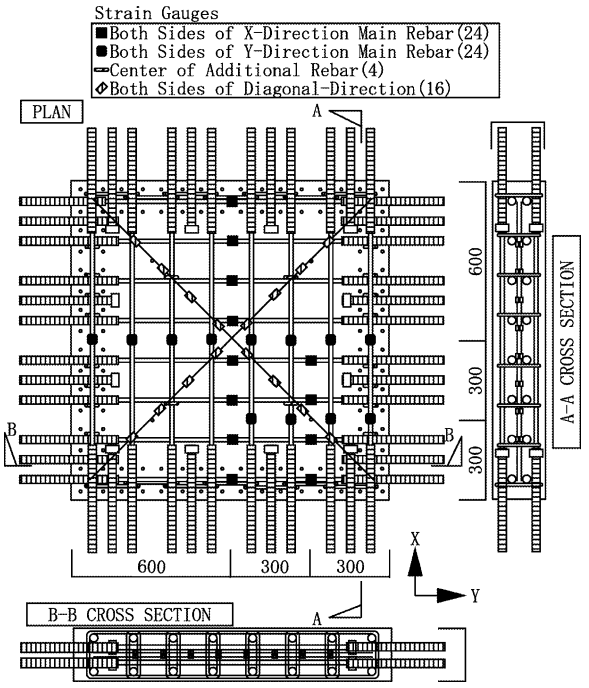

Fig. 2. Rebar arrangement.

2.3. Rebar arrangement

Rebar arrangement of the specimen is shown in Fig. 2. The main rebar arrangement is double and orthogonal with 150-mm pitch. Shear bars resisting out-of-plane shear are also arranged in the center of the specimen, so that the reinforcement ratio becomes the same as that of the prototype. Furthermore, at the outside of the specimen, shear bars are also arranged to prevent a local failure during the test.

2.4. Material properties

Design strength of the concrete is 30 MPa, and the yielding strength of the rebar is 345 MPa. The material properties of the concrete and rebar obtained by material tests are listed in Table 2. Notation such as D13+1.5 means that the diameter of the specimen rebar is 13 mm and constant axial stress of 1.5 MPa in tension is applied.

3. Loading plan

3.1. Loading test setup

The loading test setup is shown in Fig. 3(a and b), respectively. It consists of the reaction frame, loading rods made of high strength steel, and loading jacks. Tension loads are applied by four 1000 KN jacks placed outside the reaction frame. Compression loads are applied by four 1000 KN jacks placed inside the reaction frame. Shear loads are applied by four 5000 KN jacks through high strength steel rods.

3.2. Loading program

The loading program of this test is shown in Fig. 4(a and b), respectively. At the first stage of loading, the specimen is tensioned up to 3.0 MPa to generate 'horizontal' parallel cracks. Next, the tension loads are unloaded and the specific axial stress shown in Table 1 is applied. Then, holding the axial stress constant, shear stress is cyclically applied increasingly up until concrete failure. The loading is firstly controlled by stress up until shear cracking, then controlled by strain up until either failure or the shear strain reaches at 1000 μ which is set as a measuring limit.

4. Measurement

Axial, shear stresses, and strains of the RC plate specimen and rebar strains were measured during the test. Furthermore, crack patterns were checked by visual inspection and marked as a record. Stresses were estimated by the values of load cells attached to the loading jacks. Strains of the specimen were estimated by the values of displacement transducers attached on the both sides at the center of the specimen. The transducer arrangement is shown in Fig. 5. The rebar strain was measured directly by the foil strain gauges attached on the both sides of the rebar.

Table 2
Material properties

Specimen name	Age (day)	Compressive strength f_c' (MPa)	Strain at maximum stress ε_c' (μ)	Young's modulus E_c (GPa)	Poisson's ratio ν
Concrete					
D13+1.5	182	22.8	2414	21.0	0.185
D13±0.0	224	25.2	1969	21.8	0.171
D13−1.5	210	24.0	1988	21.2	0.201
D16+3.0	234	23.7	2182	21.9	0.172
D16+1.5	275	26.7	2116	25.1	0.189
D16+0.75	289	26.6	2130	23.2	0.168
D16±0.0	303	26.3	2094	22.7	0.189
D16−1.5	344	30.2	2307	24.8	0.165
D16−3.0	315	26.7	2128	24.2	0.166
D22+1.5	35	31.8	2668	26.7	0.189
D22±0.0	28	30.8	2408	26.8	0.165
D22−1.5	49	32.5	2128	26.6	0.166
Rebar name	Young's modulus E_s (GPa)	Reinforcing ratio ρ_n (%)	Yield strength f_y (MPa)	Tensile strength f_t (MPa)	
Rebar					
D13	193.2	0.84	354.7	537.9	
D16	193.2	1.32	372.8	581.1	
D22	193.7	2.58	373.7	572.7	

5. Test results and investigation

5.1. Stress–strain relationship

The representative normal stress f-normal strain ε relationship is shown in Fig. 6(a), for the D22+1.5 specimen. And the representative shear stress v-shear strain γ relationships are shown in Fig. 6(b–d). The shear stresses of the specimen at shear cracking v_c, rebar yielding v_y, and ultimate shear stress v_u are shown with symbols ●, ○ and ▼ in the figures. In Fig. 6(b–d), shear stresses at rebar

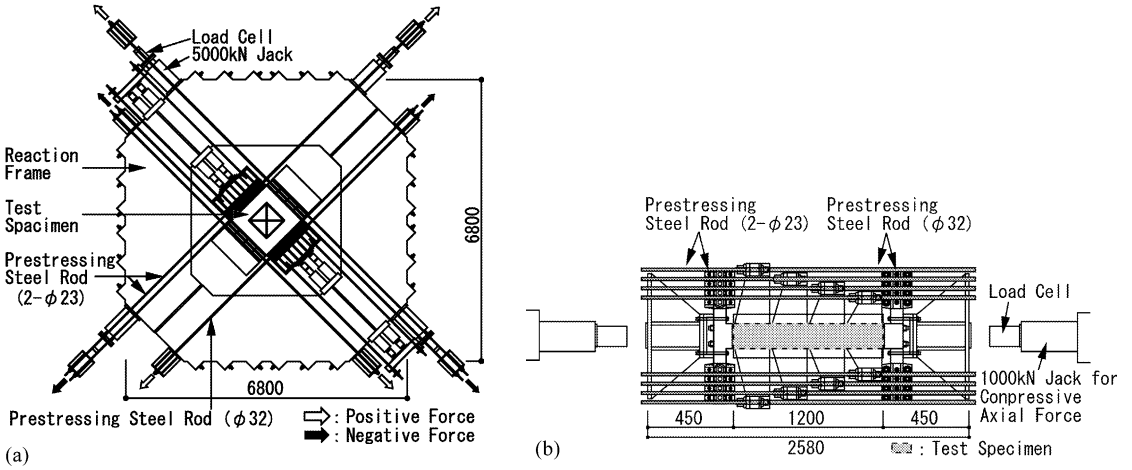

Fig. 3. (a) Loading setup (plan); (b) loading setup (elevation).

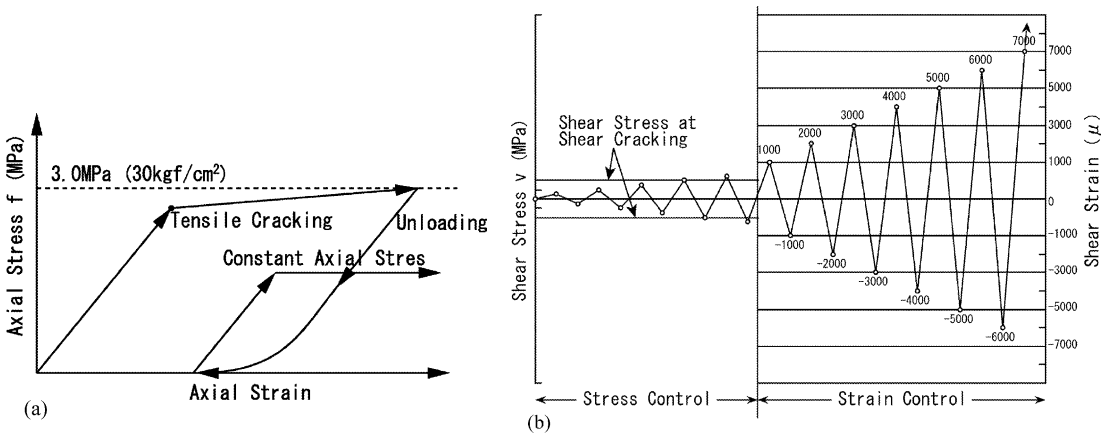

Fig. 4. (a) Loading program (axial stress); (b) loading program (shear stress).

yielding v_y (cal) and ultimate shear stress v_u (cal), calculated by Eqs. (1) and (2) are also shown by dotted and dashed lines.

In Fig. 6(b), v_u agrees with v_u (cal). On the other hand, in Fig. 6(c and d), v_u values do not agree with v_u (cal) values. Since these equations assume the concrete does not crash prior to the rebar yielding or breaking, they do not estimate the shear stress correctly in case of the assumption not being satisfied.

$$v_y(\text{cal}) = \sqrt{\rho_n f_y(\rho_n f_y - f_0)} \quad (1)$$

$$v_u(\text{cal}) = \sqrt{\rho_n f_t(\rho_n f_t - f_0)} \quad (2)$$

where v_y (cal) is the shear stress at rebar yielding calculated; v_u (cal), ultimate shear stress calculated; f_y, rebar yield stress; f_t, rebar tensile strength; f_0, axial stress applied; and ρ_n is the reinforcing ratio.

5.2. Crack patterns

Crack patterns of the specimen D13+1.5 are shown in Fig. 7(a–d) as a typical example. Fig. 7(a) shows the 'horizontal' parallel cracks. This crack pattern shows that the smeared crack model can be applied to this study. Fig. 7(b–d) show the diagonal crack developing process and the evi-

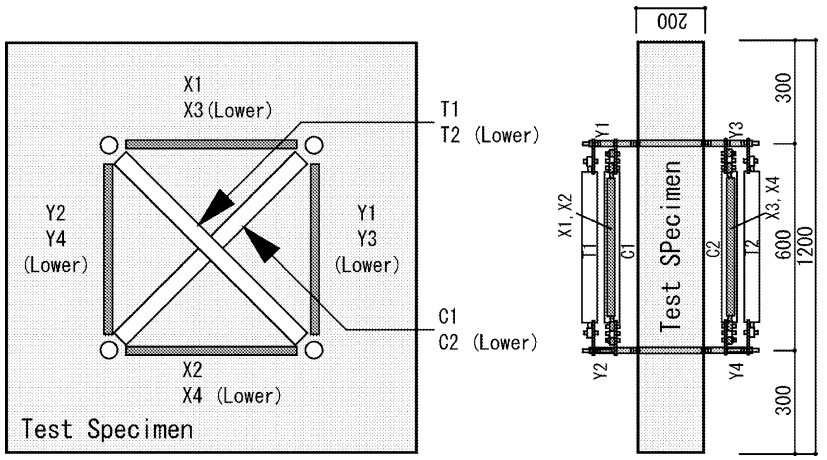

Fig. 5. Transducer arrangement.

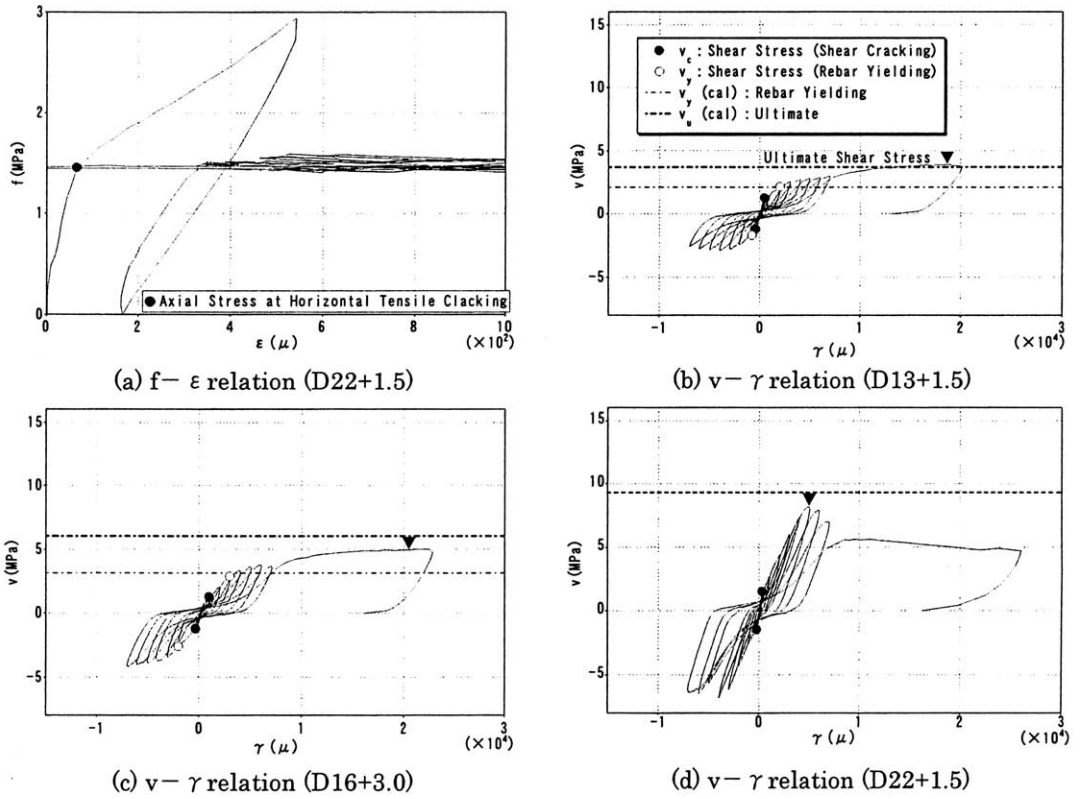

Fig. 6. Representative $f-\varepsilon$, $v-\gamma$ relation (a) $f-\varepsilon$ relation (D22+1.5), (b) $v-\gamma$ relation (D13+1.5), (c) $v-\gamma$ relation (D16+3.0), (d) $v-\gamma$ relation (D22+1.5).

dences of proper shear stress distributions, as there are no crack concentrations.

5.3. Test results

5.3.1. Measurement results

Major measurement results are listed in Table 3. The tension and shear stresses at initial horizontal and shear cracking, ${}_{n}f_c$ and v_c, were based on the visual inspection. The shear stress at rebar yielding v_y was estimated based on the rebar material test. The ultimate shear stress v_u was estimated as the maximum stress from the $v-\gamma$ relationship of each test. Initial stage shear modulus G_I was estimated from the least square method applied to the v and γ values in the region between the origin and v_c. G_I is a simple index showing the representative shear modulus of the specimen.

5.3.2. Normalization of the measurement results

${}_{n}f_c$ and v_c were normalized by the concrete tensile strength f_{ct} to have ${}_{n}f_c/f_{ct}$ and v_c/f_{ct} to eliminate the effect of the deviation in concrete strength. On the other hand, v_y and v_u were normalized by $\rho_n f_y$ to have $v_y/\rho_n f_y$ and $v_u/\rho_n f_y$ to provide stress levels. G_I was normalized by the concrete elastic shear modulus G_o from the material test to provide the initial stage shear modulus reduction factor G_I/G_o.

Concerning ${}_{n}f_c/f_{ct}$ and v_c/f_{ct}, higher reinforcing specimens show higher values. Furthermore, axially compressive loaded specimens show higher v_c/f_{ct} values than those loaded in tension. Concerning $v_y/\rho_n f_y$ and $v_u/\rho_n f_y$, axially compressive loaded specimens show higher values than tension loaded ones. Those tendencies could be caused by the change in stiffness of the specimen by the reinforcing or axial loading.

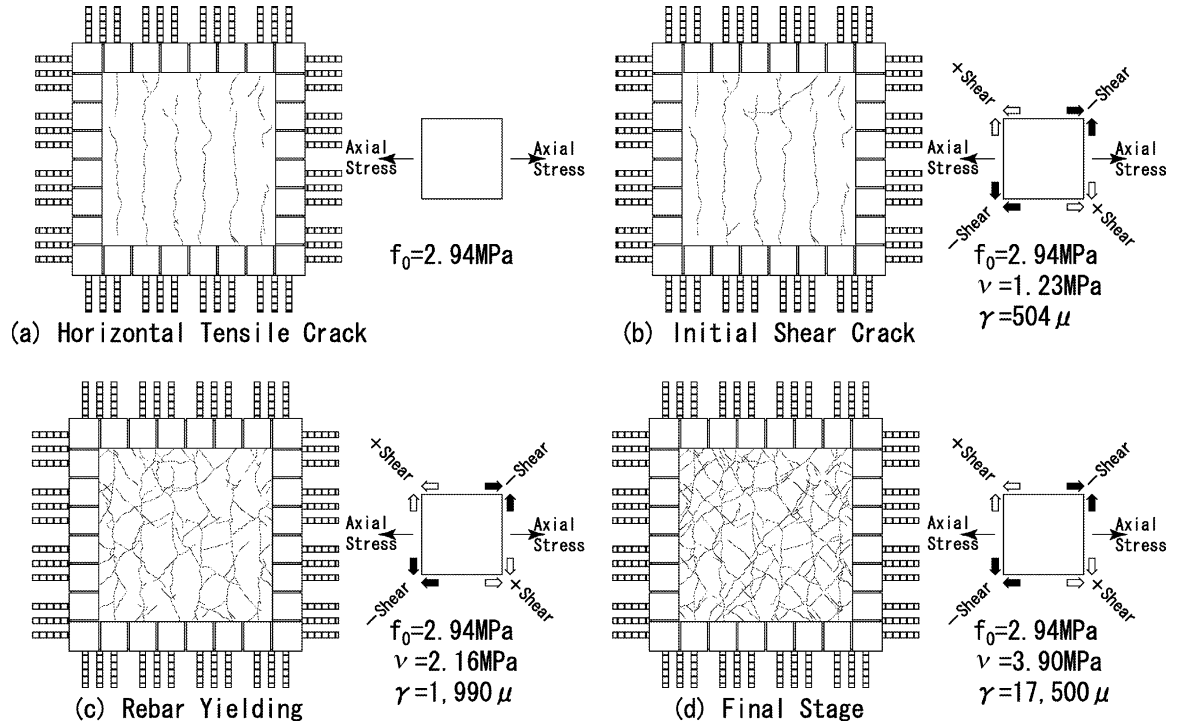

Fig. 7. Crack pattern (D13+1.5).

On the other hand, higher reinforcing specimens show lower $v_u/\rho_n f_y$. This could be caused by the change in failure mode of the specimens. As long as the concrete does not crash prior to the rebar breaking, $v_u/\rho_n f_y$ increases proportionally to the increase of the reinforcement ratio. However, if the assumption is not satisfied, the specimen could fail by concrete crash at a lower stress level.

5.3.3. *Influence of axial stress and reinforcement ratio on G_I/G_o*

The relationships between G_I/G_o and axial stresses, reinforcement ratios are shown in Fig. 8. The maximum value was 84% for D13−1.5; the minimum was 17% for D16+3.0. G_I/G_o was strongly dependent on the axial stresses applied, however, the influence of the reinforcement ratios was small.

6. Development of the constitutive model

6.1. *Concept of applying the constitutive model to the FEM analysis technique*

The constitutive model will be applied to the analysis of shear walls in NPP buildings. The feature of shear walls is being governed by shear behavior and under plane stress conditions. So, the constitutive model is to be applied to the third row, third line term of the D-matrix of the plane stress element used in FEM. As shown in Eq. (3), this term defines the shear modulus G_{cr}. In this study, the stress-strain relationship was handled in the incremental form shown in Eq. (4), because of the convenience of the analytical procedure. Therefore, G_{cr} was expressed in the form of $dv_{cr}/d\gamma_{cr}$. This term corresponds to the $dv_{cr}/d\gamma_{cr}$ derived from the test.

Table 3
Test results

Specimen name	Horizontal tensile crack				Shear crack			Rebar yield			Ultimate shear stress			Initial stage shear modulus G_I (GPa)	Concrete elastic shear modulus G_0 (GPa)	Shear modulus reduction factor G_I/G_0 (%)
	${}_nf_c$ (MPa)	f_{ct} (MPa)	${}_nf_c/f_{ct}$	${}_n\varepsilon_c$ (μ)	v_c (MPa)	v_c/f_{ct}	γ_c (μ)	v_y (MPa)	$v_y/\rho_n f_y$	γ_y (μ)	v_u (MPa)	$v_u\rho_n f_y$	γ_u (μ)			
D13+1.5	1.87	1.77	1.06	118	1.23	0.69	504	2.16	0.72	1990	3.90	1.31	17 500	2.71	8.86	31
D13±0.0	1.67	1.54	1.08	87	1.72	1.12	648	3.12	1.05	3010	4.53	1.52	23 400	5.09	9.31	55
D13−1.5	1.33	1.26	1.06	52	1.95	1.55	280	4.16	1.39	4000	5.08	1.70	20 000	7.61	9.04	84
D16+3.0	1.61	1.33	1.21	144	1.24	0.93	1010	2.88	0.59	3010	4.94	1.00	20 000	1.57	9.34	17
D16+1.5	1.48	1.14	1.30	146	1.24	1.09	474	4.47	0.91	4000	6.08	1.24	20 100	3.77	10.56	36
D16+0.75	1.29	1.16	1.11	61	1.45	1.25	383	4.72	0.96	4000	6.34	1.29	18 100	5.03	9.93	51
D16±0.0	1.39	1.19	1.17	86	1.58	1.33	430	5.11	1.04	4000	6.49	1.32	14 500	5.60	9.55	59
D16−1.5	1.53	1.41	1.09	56	1.98	1.40	462	5.47	1.11	4000	7.31	1.48	13 100	6.08	10.64	57
D16−3.0	1.41	1.32	1.07	40	1.93	1.46	392	6.2	1.26	4030	7.52	1.52	11 000	6.52	10.38	63
D22+1.5	1.46	1.14	1.28	67	1.48	1.30	345	–	–	–	8.16	0.85	5030	5.26	11.23	47
D22±0.0	1.47	1.15	1.28	71	2.03	1.77	498	–	–	–	8.74	0.91	4830	5.57	11.50	48
D22−1.5	1.66	1.21	1.37	98	2.19	1.81	433	–	–	–	9.34	0.97	5010	7.54	11.41	66

${}_nf_c$, Axial stress at horizontal cracking; v_y, shear stress at rebar yielding; G_0, $E_c/2(1+\nu)$; ${}_n\varepsilon_c$, axial strain at horizontal cracking; γ_y, shear strain at rebar yielding; E_c, concrete young's modulus; v_c, shear stress at shear cracking; v_u, ultimate shear stress; ν, concrete poisson's ratio; γ_c, shear strain at shear cracking; γ_u, ultimate shear strain at v_u f_c', compressive strength of concrete; f_{ct}, tencile strength of specimen concrete; G_I, initial stage shear stiffness; ρ_n, reinforcing ratio; +, axial tension; −, axial compression; f_y, rebar yield stress.

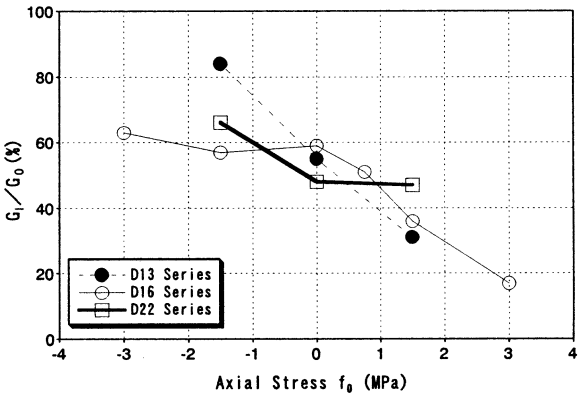

Fig. 8. Shear modulus reduction factor-axial stress.

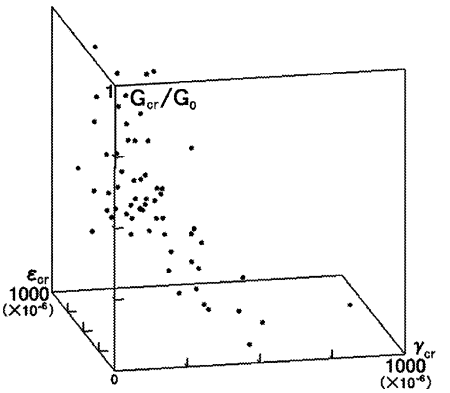

Fig. 10. $G_{cr}/G_o-\gamma_{cr}\varepsilon_{cr}$ relation.

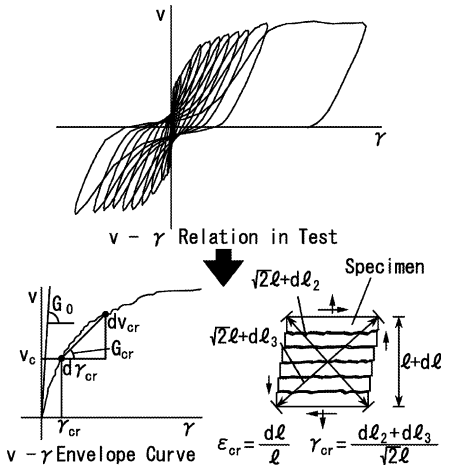

Fig. 9. G_{cr} estimation.

The data of $dv_{cr}/d\gamma_{cr}$ were derived from the envelop curve of the $v-\gamma$ relationship in the region between the origin and v_c. At that region, basically, there were only horizontal parallel cracks in the specimen. Since stresses must be transferred through these cracks, the data concerning the shear transfer could be collected under ideal conditions. The envelop $v-\gamma$ curve in the region was decomposed to $dv_{cr}/d\gamma_{cr}$ as in Fig. 9, that was defined as the shear modulus G_{cr}. In the procedure, $v-\gamma$ were expressed as $v_{cr}-\gamma_{cr}$ because the test was conducted on the pre-cracked specimen. In order to smooth G_{cr}, the envelop curve was smoothed by taking every third sequential values prior to the evaluation. And G_{cr} was normalized

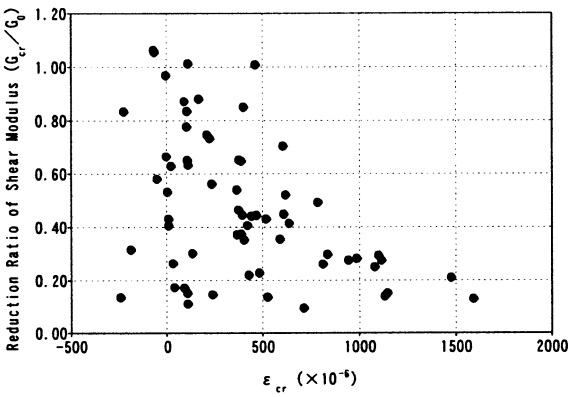

(a) Constant γ_{cr} View

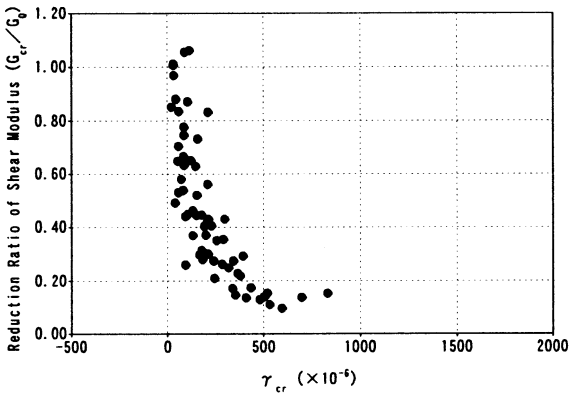

(b) Constant ε_{cr} View

Fig. 11. Side view of Fig. 10(a) constant γ_{cr} view, (b) constant ε_{cr} view.

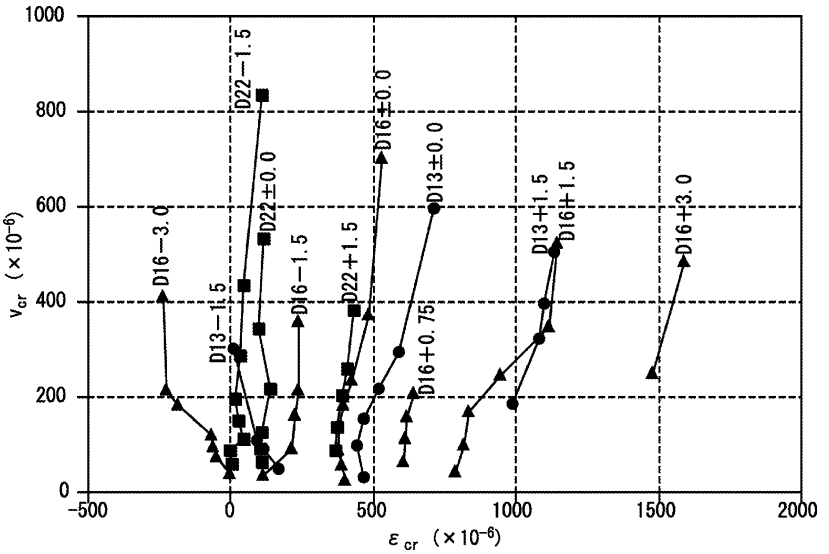

Fig. 12. $\varepsilon_{cr}-\gamma_{cr}$ relation in test.

by elastic shear modulus G_o to have the shear modulus reduction factor G_{cr}/G_o.

$$\begin{bmatrix} f_{cr} \\ f_p \\ v_{cr} \end{bmatrix} = \begin{bmatrix} 0 & 0 & 0 \\ 0 & E_c & 0 \\ 0 & 0 & G_{cr} \end{bmatrix} \begin{bmatrix} \varepsilon_{cr} \\ \varepsilon_p \\ \gamma_{cr} \end{bmatrix} \tag{3}$$

$$\begin{bmatrix} df_{cr} \\ df_p \\ dv_{cr} \end{bmatrix} = \begin{bmatrix} 0 & 0 & 0 \\ 0 & E_c & 0 \\ 0 & 0 & G_{cr} \end{bmatrix} \begin{bmatrix} d\varepsilon_{cr} \\ d\varepsilon_p \\ d\gamma_{cr} \end{bmatrix} \tag{4}$$

where E_c is the elastic modulus of concrete; G_{cr}, Shear modulus of cracked concrete; cr, direction perpendicular to the crack plane; and p is the direction parallel to the crack plane.

6.2. Development of the constitutive model

6.2.1. Relationship between formulation and test conditions

By examining the test dada, it was apparent that G_{cr}/G_o depends on both normal strain ε_{cr} and shear strain γ_{cr}, respectively, as in Fig. 10. Side views of the figure are shown in Fig. 11(a and b). From the figures, it was apparent that the measured strains fall on the region as $-250 < \varepsilon_{cr} < 1600$ μ, $0 < \gamma_{cr} < 800$ μ and G_{cr}/G_o decreases with the increase of strain. Therefore, the basic formula Eq. (5) was developed. Since ε_{cr} was not changed

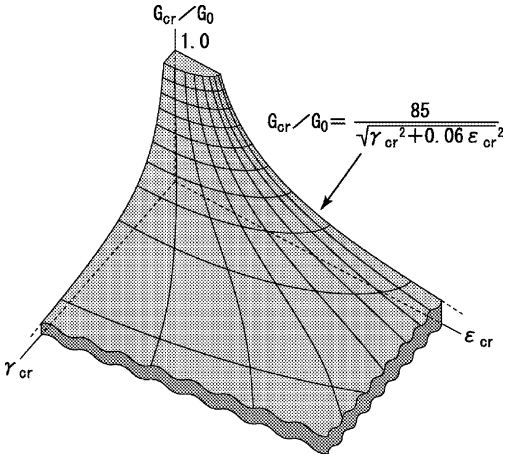

Fig. 13. Configuration of Eq. (8).

in comparison γ_{cr} in the test, the term $d\varepsilon_{cr}/d\gamma_{cr}$ was small as in Fig. 12. Therefore, G_{cr} actually equals to $\partial v_{cr}/\partial\gamma_{cr}$ as in Eq. (6).

$$G_{cr} = \frac{dv_{cr}}{d\gamma_{cr}} = \frac{\partial v_{cr}}{\partial \varepsilon_{cr}} \frac{d\varepsilon_{cr}}{d\gamma_{cr}} + \frac{\partial v_{cr}}{\partial \gamma_{cr}} \tag{5}$$

$$G_{cr} = \frac{dv_{cr}}{d\gamma_{cr}} = \frac{\partial v_{cr}}{\partial \gamma_{cr}} \tag{6}$$

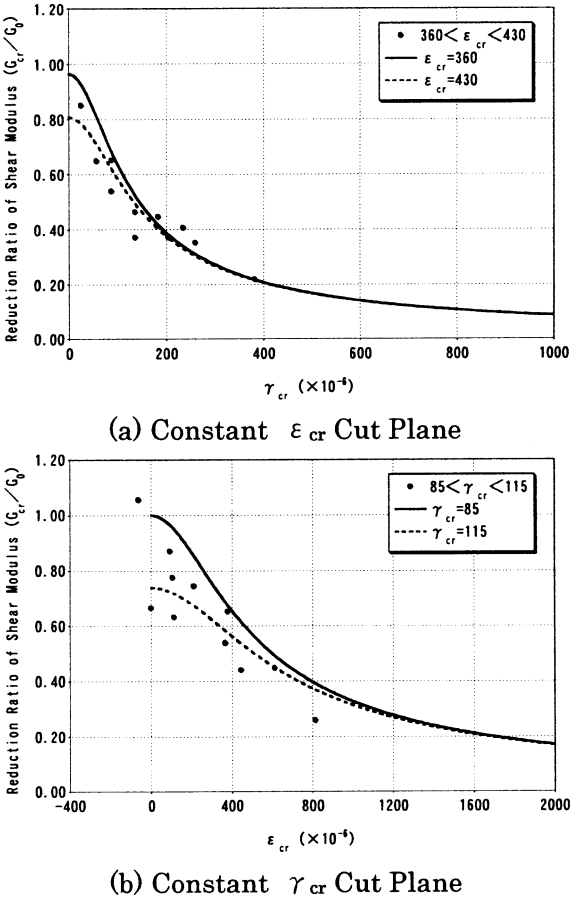

Fig. 14. G_{cr}/G_o between proposed model and test, (a) constant ε_{cr} cut plane, (b) constant γ_{cr} cut plane.

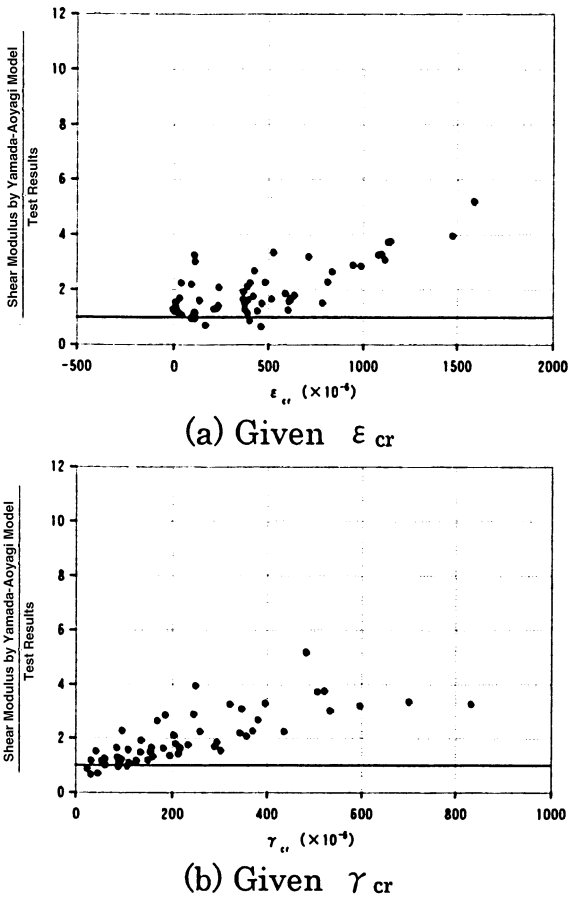

Fig. 15. Shear modulus between Yamada–Aoyagi model and test, (a) given ε_{cr}, (b) given γ_{cr}.

6.2.2. Proposal of the shear transfer constitution model

From the data scattering in Fig. 10, G_{cr}/G_o was thought to be expressed as a certain function of ε_{cr} and γ_{cr}. In order to find the proper function, a function in Eq. (7) was postulated. A and B are the unknown parameters. By the multi regression analysis, these unknown parameters were determined in Eq. (8). In the analysis, ε_{cr} in compression was excluded assuming the crack was closed and $\varepsilon_{cr} = 0$. Additionally, G_{cr}/G_o values greater than 1.0 were treated as 1.0 so that it formed an upper limit. Since the correlation coefficient of the regression analysis was $R = 0.777$, Eq. (8) was able to predict test results fairly well. The configuration of this function is shown in Fig. 13. This equation was proposed as the shear transfer constitution model for pre-cracked RC plate that modeled the NPP building shear wall. The agreement of the estimation results of Eq. (8) with test data are shown in Fig. 14(a and b). They show the cut planes from Fig. 13 setting ε_{cr} and γ_{cr} constant. From the figures, it was apparent that the estimation results of Eq. (8) agree reasonably well with test data.

$$\frac{G_{cr}}{G_o} = \frac{A}{\sqrt{\gamma_{cr}^2 + B\varepsilon_{cr}^2}} \tag{7}$$

where A and B are the unknown parameters.

$$\frac{G_{cr}}{G_o} = \frac{85}{\sqrt{\gamma_{cr}^2 + 0.06\varepsilon_{cr}^2}} \tag{8}$$

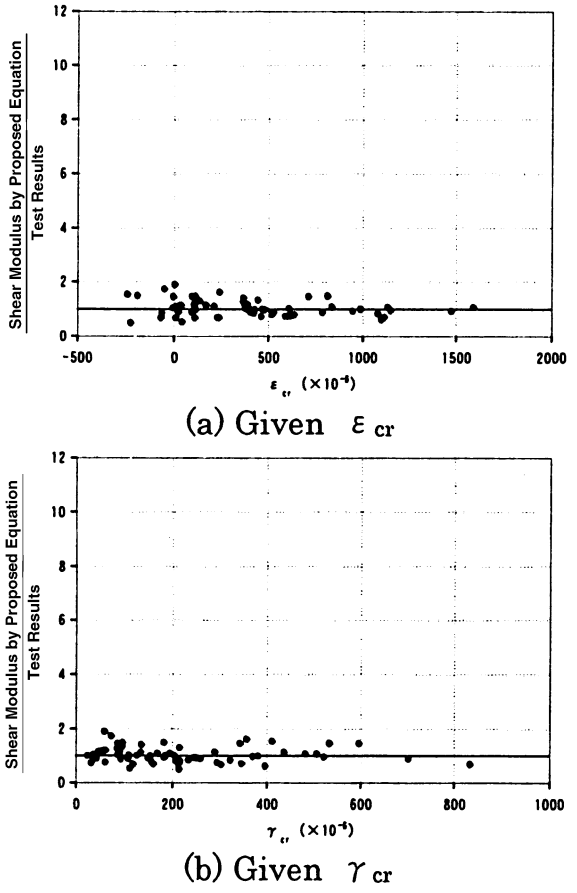

Fig. 16. Shear modulus between proposed model and test (a) given ε_{cr}; (b) given γ_{cr}.

where G_{cr} is the tangential shear modulus at crack surface; G_o, elastic shear modulus; γ_{cr}, shear strain (μ); ε_{cr}, normal strain perpendicular to crack (μ); $G_{cr} \leq 1.0\ G_o$, $\varepsilon_{cr} = 0$ in case of ε_{cr} is in compression.

7. Applicability of the proposed model

7.1. Comparison between test data and estimation results by existing and proposed models

The relationship between G_{cr} and ε_{cr} and γ_{cr} from the test was compared with the estimation results of an existing model. Yamada and Aoyagi (1983) model was selected as a representative since this was known as the smeared crack model. The model formula is shown in Eq. (9).

$$G_{cr} = \frac{36}{\varepsilon_{cr}} \tag{9}$$

where G_{cr} is the secant shear modulus at crack surface; and ε_{cr} is the normal strain perpendicular to crack.

The crack pattern in Fig. 7(a) shows that the smeared crack model concept could be applied to this test. Given ε_{cr} and γ_{cr} values from the test, corresponding G_{cr} values were estimated by the model and compared with test data in Fig. 15. As the model evaluated the secant modulus, it was evaluated in every measuring step of the test. As a whole, the model provided greater values than the test data in greater strain domain.

On the other hand, given ε_{cr} and γ_{cr}, tangential G_{cr} values were estimated by the proposed model and compared with the test data in Fig. 16. The correlation of the estimation results and the test data in Fig. 16 is better than those in Fig. 15.

7.2. Comparison between loading test and analysis results

The proposed model was incorporated to a nonlinear FEM analysis code. Using this code, a box type concrete shear wall specimen was analyzed and compared with the loading test results of another project (Endo et al., 1985). Analyses were also carried out using the simple model of G_{cr}/G_o to be constant, 0.125 and 0.8. The conditions reflected on the analysis are listed in Table 4 (Fafitis and Shah, 1985; Darwin and Pecknold, 1977; Izumo et al., 1987; Kupfer and Gerstle, 1973).

A test was conducted by horizontal two way sequential loading from 'y' to 'x' direction with the test specimen shown in Fig. 17. In the first stage, the specimen was horizontally loaded in the 'y' direction up to overall shear crack occurring under no axial loads. At this stage, shear stress was around 7.0 MPa ($=4.0\sqrt{f_c(\mathrm{kgf\ cm^{-2}})}$, f_c is concrete compressive strength). After unloading, in the second stage, the specimen was horizontally loaded cyclically up to the ultimate strength in 'x' direction under constant axial stress 1.96 MPa.

Table 4
Conditions reflected on analysis

	Overview
Element	Sell Element, 4 Nodal Point
Crack Model of Concrete	Active Crack Model
Stress—Strain Model	Concrete : Uni-axial strength - strain curve Reinforcement: Bi - linear Compression Before Compressive Strength : Fafitis - Shar Model After Compressive Strength : Darwin - Pecknold Model Tension Before Crack : Elastic After Crack : Tension Stiffning (Izumo Model) 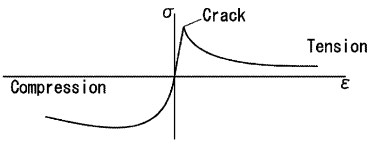
Yield・Failure Criteria	Compression—Compressin : Kupfer - Gerstle Tension—Compression : Darwin - Pecknold Tension—Tension : Prinsipal Stress ≧Uni-axial Tensile Strength
Bond Slip Model	Without Slip
Shear Transfer Model at Crack Surface	・Reduction Factor of Shear Stiffness (β=0.125 , 0.8) ・Proposed Equation

The relationships between applied horizontal load and deflection angle are shown in Fig. 18. In the figure, rotation angle measured at the bottom of the wall was drawn from deflection angle at every step to adjust the boundary conditions between test and analysis.

From the figures, several important points were clarified.

7.2.1. At the first loading stage

Analysis results agreed well with the test results. As cracks initiated in this stage, analysis results were not influenced by the difference between proposed and simple models.

7.2.2. At the second loading stage

As a whole, analysis results by the proposed model agreed with the test results fairly well. On the other hand, the results by the simple model did not agree with the test results. This shows the proposed model could promote the analytical accuracy.

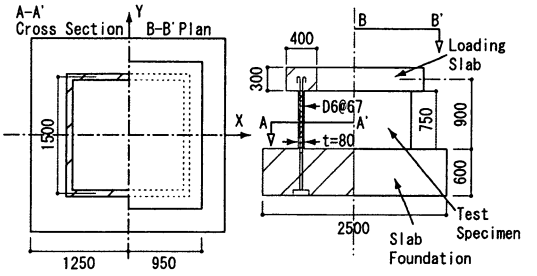

Fig. 17. Box type shear wall specimen.

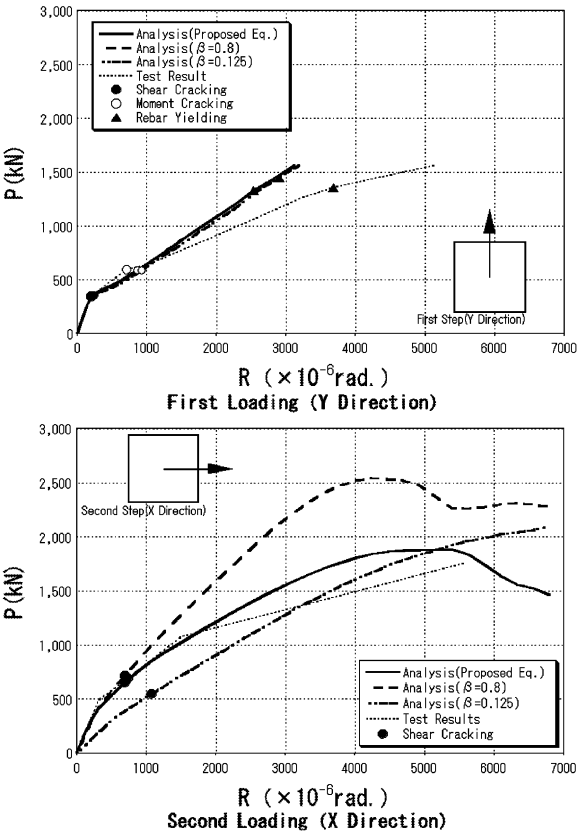

Fig. 18. Comparison between analysis and test in P–R relation.

8. Conclusions

The shear transfer constitutive model was developed from the test data, obtained by loading

combined axial and cyclic shear force to 12 pre-cracked RC plates. The major results of this study are shown below. (1) Initial stage shear modulus reduction factor G_I/G_o was strongly influenced by axial stress applied to the pre-cracked RC plate specimen, on the other hand, the influence of the reinforcement ratio was small. (2) By conducting multi regression analysis, shear modulus reduction factor, G_{cr}/G_o, was expressed as the function of ε_{cr} and γ_{cr}. The function was proposed as the shear transfer constitutive model for the shear wall. (3) Comparing test data with the estimation results of the proposed and existing models, it was apparent that the proposed model could evaluate the G_{cr}/G_o ratio more accurately than the existing model. (4) The proposed model was incorporated into the nonlinear structural analysis code. The behavior in the two horizontal directions of the box type RC shear wall specimen was analyzed and compared with test results. From the comparison, it was apparent that the proposed model could improve the analytical results. And the model will be effective when it is applied to the nonlinear crack analysis.

Acknowledgements

This study was performed by NUPEC as a part of the 'Model Tests of Multi-Axis Loading on RC Shear Walls' project commissioned by the Ministry of Economy, Trade and Industry (METI) of Japan. Technical issues have been discussed in the Advisory Committee on the project established within NUPEC. The authors wish to express their gratitude to all the members of committee for their encouragement and valuable discussions and co-operation.

References

Darwin, D., Pecknold, D.A., 1977. Nonlinear biaxial stress–strain law for concrete. Journal of the Engineering Mechanics Division, ASCE, vol. 103. No. EM2, pp. 229–241.

Endo, A., Watabe, M., Narikawa, T., Kato, M., Kusama, K., 1985. Experimental studies on the seismic behavior of R/C box walls under two-directional loadings (Part 1: Two-Step Loading Tests). Summaries of Technical Papers of Annual Meeting, Architectural Institute of Japan, pp. 827–828.

Fafitis, A., Shah, S.P., 1985, Lateral reinforcement for high-strength concrete columns. ACI Publication, No. SP-87, pp. 213–232.

Habasaki, A., Kitada, Y., Yamada, M., Nisikawa, T., 2000. Constitutive model of shear transfer for pre-cracked RC plate subjected to combined axial and shear stress. Journal of Structural Construction Engineering, Architectural Institute of Japan, No. 538, 2000, pp. 139–145.

Izumo, J., Shima, H., Okamura, H., 1987. Analytical model for reinforced concrete panel elements subjected to in-plane forces. Concrete Journal, Japan Concrete Institute, No. 87.9–1, pp. 107–120.

Kitada, Y., Nishikawa, T., Maekawa, K., Umeki, K., Yamada, M., Kamimura, K., 1999. Shear behavior of pre-cracked RC plates subjected to combined axial and shear stress. Transaction of the Fifteenth Structural Mechanics in Reactor Technology, vol. VI. Seoul, pp. 325–332.

Kupfer, H.B., Gerstle, K.H., 1973. Behavior of concrete under biaxial stress. Journal of the Engineering Mechanics Division. ASCE, vol. 99, No. EM4, pp. 853–866.

Yamada, K., Aoyagi, Y., 1983. Shear transfer across crack, Proceedings of JCI Second Colloquium on Shear Analysis of RC Structures, pp. 19–28.